Geomechanics and Engineering, *Vol. 43, No. 1 (2025) 69-74*
https://doi.org/10.12989/gae.2025.43.1.069

Study on the equivalent stiffness of limestone particles in single particle crushing test based on particle strength and specific fracture energy

Buxueyan Wang[1], Zhiyong Liu[3], Jiangu Qian*[1,2] and Ilhan Chang[4]

[1]*Department of Geotechnical Engineering, Tongji University, Shanghai, 200092, China*
[2]*State Key Laboratory of Disaster Reduction in Civil Engineering, Tongji University, Shanghai, 200092, China*
[3]*Shanghai Key Laboratory of Rail Infrastructure Durability and System Safety, Tongji University, Shanghai, 201804, China*
[4]*Department of Civil Systems Engineering, Ajou University, Suwon-si, 16499, Republic of Korea*

(*Received June 17, 2025, Revised September 30, 2025, Accepted October 2, 2025*)

Abstract. Particle breakage can alter the gradation of soil, reduce the interparticle contact friction induced by shear, and serve as a primary cause of deformation in geomaterials, significantly influencing their engineering mechanical properties. The single-particle crushing test is an essential test method for investigating particle breakage and strength. However, merely analyzing particle strength neglects the deformation information during the crushing process, leading to an inability to accurately characterize the strain state before the particle's overall breakage. In this study, single-particle crushing tests were designed and conducted to analyze the particle strength and specific fracture energy of limestone particles. Based on the analytical results, an equivalent stiffness was formulated. By introducing the concept of equivalent stiffness, the distribution of specific fracture energy was transformed into a particle strength distribution. The validity and reliability of this conversion method were verified, demonstrating its effectiveness in statistically characterizing different stress-path features of particles. This study reveals that the equivalent stiffness of 10-20 mm Baihetan limestone particles in single-particle crushing test is 4.7×10^6N/m. This result offers a reference value for associated numerical modeling and can inform the corresponding engineering design.

Keywords: equivalent stiffness; particle strength; single-particle crushing test; specific fracture energy

1. Introduction

Particle breakage can alter the soil gradation, reduce interparticle contact friction induced by shear, and serve as a primary mechanism for deformation in geomaterials, significantly influencing their engineering mechanical properties (Sowers 1965, Marsal 1973, Penman 1976, Veiga 1983). The extent of particle breakage is governed by multiple factors, including grain size distribution (GSD), particle strength, geometric morphology, weathering degree, moisture content, and stress levels. Based on single-particle test data, Weibull (1951) proposed a statistical method to characterize the strength and variability of brittle materials, which effectively describes the magnitude and dispersion of sample strength in statistical processes, offering a robust representation of the probability distribution of brittle particle fracture strength. Numerous scholars have adopted the Weibull distribution to investigate single-particle strength (Marsal 1972, Lee 1992, Nakata 1999, Qing 2022, Li 2024, Meng 2022).

In these studies, single-particle strength is typically determined through uniaxial compression tests, where a particle is subjected to compressive force between two parallel rigid plates until fracture occurs. According to Griffith's theory of brittle materials (Griffith 1921), particle strength is influenced by internal microstructure, exhibiting an inverse proportionality to the square root of the initial microcrack length. Consequently, the distribution of internal microcracks and the loading configuration directly affect particle strength, leading to considerable data scatter in single-particle crushing tests. This is particularly evident when analyzing stress paths, as the complex loading history makes it challenging to directly extract the compressive modulus from individual particle compression curves. Moreover, when only fracture strength is statistically analyzed, the stress-strain data throughout the compression process remain unprocessed, rendering the results incapable of reflecting the stress-path characteristics of particles. This oversight results in the neglect of strain behavior during particle breakage, hindering an accurate description of the deformation process. Such limitations are apparent in certain numerical simulations (Jiang 2014, Gong 2021), where particle stiffness is often treated as a calibration parameter rather than experimentally derived property, casting doubt on its physical validity. Many scholars have conducted research on the breakage of geotechnical materials, but have not been able to effectively solve the deformation problem during particle breakage (Tu 2022, Xi 2023, Zhou 2016, Li 2023, Golewski 2024, Golewski 2025). Thus, it is imperative to introduce a parameter that simultaneously captures both stress and strain (or stiffness) characteristics to describe particle breakage comprehensively.

Fracture energy serves as an effective metric to characterize particle breakage, as it incorporates stress-path

*Corresponding author, Professor
E-mail: qianjiangu@tongji.edu.cn

ISSN: 2005-307X (Print), 2092-6219 (Online)

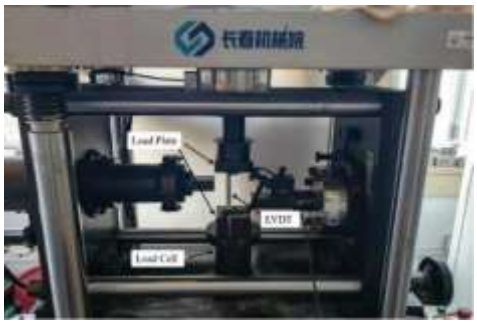

Fig. 1 High-accuracy loading instrument

Table 1 Basic parameters of the sample

Number	Mass(g)	Width(mm)	Length(mm)	Height(mm)
3	0.97	11.40	12.00	6.80
15	5.31	16.94	17.50	11.74
17	2.87	11.27	22.41	7.93

information and reflects both stress and strain responses during fracture. This makes it a suitable descriptor for the breakage process, complementing particle strength analysis. Tavares (1998, 2002) investigated fracture energy distribution through impact tests, demonstrating that this approach provides a framework for integrating force and displacement characteristics. Building on this work, Wang (2025) designed single-particle crushing tests for limestone, refining impact-test-derived formulas to better suit quasi-static compression experiments, while also examining the influence of moisture on limestone's fracture energy dissipation.

Drawing on these advancements, this study introduces the concept of equivalent stiffness (nominal stiffness) based on characteristic strength and specific fracture energy from single-particle crushing tests, offering an approximate representation of strain evolution during particle breakage.

2. Single-particle crushing test

A single-particle crushing test was designed to elucidate the stress-strain behavior during particle breakage. The test material consisted of limestone particles with a grain size of 10–20 mm, sourced from the Baihetan Hydropower Station. Prior to testing, the particles were oven-dried at 105°C for 24 hours to ensure a consistent moisture-free state.

The experiments were conducted using a high-precision loading apparatus (Fig. 1), with a uniaxial loading rate set to 0.005 mm/s to meet quasi-static conditions (Tavares 2007). The room temperature during the loading process was 18°C, with an indoor humidity of 70%. Particle breakage was defined as occurring when the volumetric loss of the particle exceeded 10% (Gabriel 2011).

3. Mechanical data and analysis

The morphological changes before and after breakage of particle No.3 are illustrated in Fig. 2. The force-

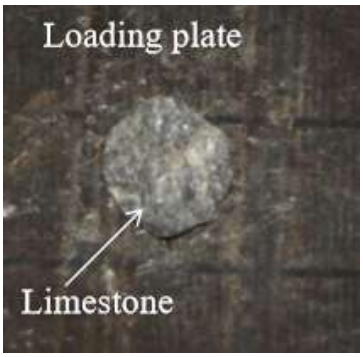

(a) Particle No.3 before breakage

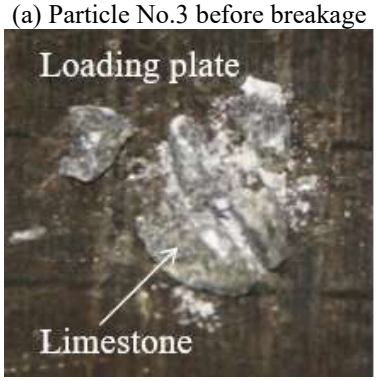

(b) Particle No.3 after breakage

Fig. 2 Morphological changes before and after breakage of particle No.3

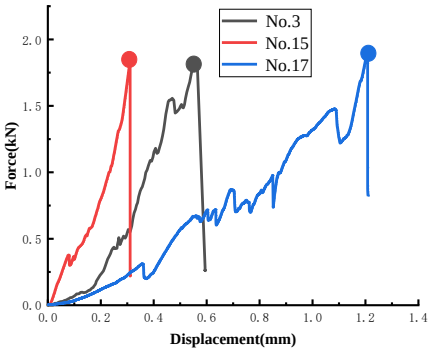

Fig. 3 Force displacement curve of the sample

displacement curve of each particle during loading was recorded by computer for subsequent data analysis.

Fig. 3 presents the force-displacement curves of particles No.3, No.15, and No.17 obtained in this test, the basic morphological parameters of these three particles are shown in Table 1. As observed, these three particles exhibited similar peak forces at failure, all approximately 1.8 kN. However, the displacements between loading plates at failure varied significantly, measuring 0.31 mm for particle No.15, 0.55 mm for particle No.3, and 1.21 mm for particle No.17 in ascending order. Consequently, relying solely on peak force cannot adequately reflect the displacement state during particle fragmentation.

Furthermore, the three curves demonstrate distinct characteristics: Particle No.15 displays a single-peak pattern with a relatively smooth curve, indicating no significant

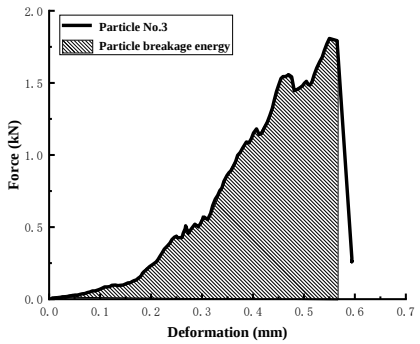

Fig. 4 Particle breakage energy

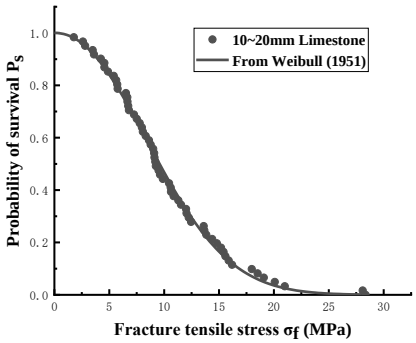

Fig. 5 Fracture tensile stress of limestone particles

localized failure prior to complete fracture. In contrast, particle No.3 exhibits a double-peak pattern, suggesting one notable localized fracture event before overall failure. The curve of particle No.17 is the most irregular, with pronounced fluctuations and a jagged morphology, implying multiple intense localized fractures preceding complete disintegration.

The variations in these curves also demonstrate that the peak force at failure cannot fully capture the stress path information of the particles. Determining a statistically reasonable stiffness parameter from individual particle curves remains a critical research challenge.

To address the limitation of peak force in reflecting stress path characteristics, this study introduces fracture energy as an auxiliary parameter to investigate particle breakage. Taking particle No.3 as an example, the area enclosed by its force-displacement curve at fragmentation and the x-axis (displacement) represents its fracture energy.

$$E = \int_0^{\Delta_c} F d\Delta \tag{1}$$

where E is the fracture energy, F is the pressure exerted on the particles, Δ is the particle deformation and Δc is the deformation at fracture.

Additional characteristics of the particle are presented in Table 1, where:

Length corresponds to the maximum Feret diameter

Height represents the minimum Feret diameter

Width denotes the maximum Feret diameter perpendicular to both height and length directions

As shown in Fig. 4, the fracture energy is calculated as the area enclosed by the force-displacement curve at particle failure and the X-axis. This value depends on the peak stress, corresponding failure displacement, and fluctuations in the curve, thereby simultaneously reflecting both the stress-strain behavior and stress path characteristics during particle breakage. Therefore, subsequent analyses will incorporate both the peak force and fracture energy distribution features of the particles.

4. Prticle strength characteristic

To quantify particle strength, the maximum tensile stress σ_f (Nakata 2001) is introduced as an evaluation parameter. Under external compressive loading, tensile stresses develop within soil particles. Fracture occurs when these tensile stresses reach the particle's bearing capacity limit. Cavarretta (2012) conducted systematic analyses of stress states in irregular particles during single-particle crushing tests and proposed the following expression

$$\sigma_f = \frac{0.225N}{d^2/4} = \frac{0.9N}{d^2} \tag{2}$$

where N is the force at particle failure and d is the particle dimension, taken as $d = (d_2 d_3)^{1/2}$, where d_2 and d_3 are the dimensions of the minimum section of the smallest circumscribable cuboid (SCC) of the particle, that is, the intermediate and minimum diameters.

The calculated data for individual particles obtained from the above equation are presented as scatter points in Fig. 5. As can be observed from the figure, soil particles, as heterogeneous brittle materials, exhibit variability in characteristic strength even among limestone particles within the same size range due to their internal structural differences.

To characterize the strength distribution of soil particles, McDowell and Bolton (2000) proposed that the relationship between particle survival probability and tensile stress should be established based on the statistical framework developed by Weibull (1951)

$$P_s = exp\left[-\left(\frac{\sigma}{\sigma_0}\right)^m\right] \tag{3}$$

where Ps represents the probability of a particle surviving under a tensile stress σ, σ_0 is the characteristic strength, defined as the stress level at which 37% of the particles in a given volume exhibit a strength equal to or greater than this value. The Weibull modulus m, is used to quantify the uniformity of particle strength, reflecting the variation in σ within a population of particles. A higher value of m indicates a reduction in the variability of particle strength.

The fitted curve using Eq. (3) is shown as the solid line in Fig. 5, with the characteristic stress (σ_0) and Weibull modulus (m) of the tested samples being 11.38 MPa and 2.13, respectively. After restructuring the functional form on both sides of Eq. (3), the Weibull distribution of the limestone particles is presented in Fig. 6. The diagonal line

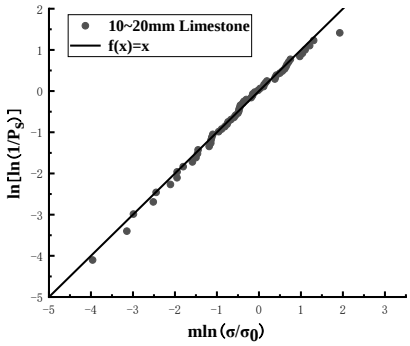

Fig. 6 Weibull distribution of limestone particles

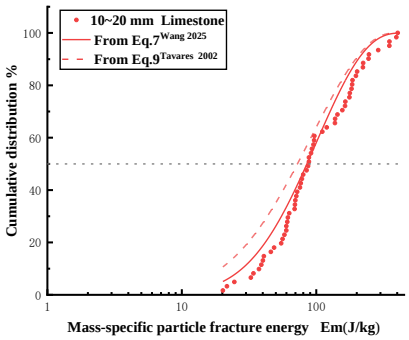

Fig. 7 Force displacement curve of the sample

in Fig. 6 represents the optimal Weibull fit, and it can be observed that most experimental data points cluster near this diagonal, indicating excellent fitting results and demonstrating good agreement with the Weibull distribution.

5. Particle energy characteristics

The fracture energy of particles can be calculated from the force-displacement curve according to Eq. (1), with its value being dependent on the stress path during particle breakage. Evidently, larger particles require greater fracture energy absorption upon breakage. Therefore, similar to particle strength, the fracture energy needs to be normalized. The specific fracture energy of each particle is defined as the ratio of its fracture energy to mass

$$E_m = \frac{E}{m} \tag{4}$$

E_m : Specific fracture energy, represents the energy required to crush each kilogram of particles.

When the external energy input of the particle is E, the probability of material breakage (P_0) is represented by Eq. (5) (Tavares 2002), where E_m* is generated by substituting the following Eq. (6) (Tavares 2002).

$$P_0(E) = \frac{1}{2}\left[1 + erf\left(\frac{ln\, E_m{}^* - ln\, E_{m,50}}{\sqrt{2\sigma^2}}\right)\right] \tag{5}$$

$$E_m{}^* = \frac{E_{m,max} E_m}{E_{m,max} - E_m} \tag{6}$$

Where:

$E_m{}^*$: Relative mass-specific fracture energy of particles

E_{m50} : Median mass-specific fracture energy of particles

σ^2: Truncate the variance of the lognormal distribution on the breakage energy

$E_{m,max}$: The maximum mass-specific fracture energy that particles can withstand (corresponds to the specific fracture energy, beyond which all particles will break in one load.)

In this equation, both E_{m50} and $E_{m,max}$ were obtained from the distribution of single-particle test results, with values of 88.19 J/kg and 403.45 J/kg respectively in the current experiments. The specific fracture energy distribution of the limestone samples is presented as scattered points in Fig. 7, where the dashed line represents the fitted curve using Eq. (6). Notably, the initial fitting results showed poor agreement, potentially attributable to: (1) the unique loading mode of single-particle crushing tests, and (2) the use of actual particle mass rather than graded particle evaluation mass in the experiments. Consequently, this study adopted the modified formula proposed by Wang (2025) as a replacement for Eq. (7). The refitted results, displayed as the solid line in Fig. 7, demonstrate significantly improved correlation.

$$E_m{}^* = \frac{\beta E_{m,max} E_m}{E_{m,max} - \beta E_m} \tag{7}$$

Where parameter β is related to the particle morphology. The value of β is in the range (0, 1], and its specific value needs to be determined by continuously adjusting β to achieve the optimal fitting effect of the equation. By examining the functional form of Eq. (7), it can be observed that when β equals 1, Eq. (7) is identical to the previous version of Eq. (6), which represents the standard spherical shape of the particle. As the difference between the particle and the spherical shape increases, the value of β approaches 0. By continuously adjusting the value of β and observing the fitting performance, the optimal value of β can be determined. For the results of this test, the best fitting performance is achieved when the morphological parameter β is set to 0.85.

6. Equivalent stiffness

Assuming particles behave as perfectly elastic bodies, the fracture energy E can be expressed as a function of the applied compressive force F. Through Eq. (5), Eq. (7), and Eq. (8), the specific fracture energy distribution shown in Fig. 7 can be transformed into a distribution of particle fracture tensile strength.

In the Weibull distribution of particle tensile strength, which is primarily governed by the characteristic strength σ_0 and Weibull modulus m, the parameter m solely quantifies the uniformity of strength distribution while the magnitude of particle strength is essentially characterized by σ_0. To facilitate comparative analysis with experimentally

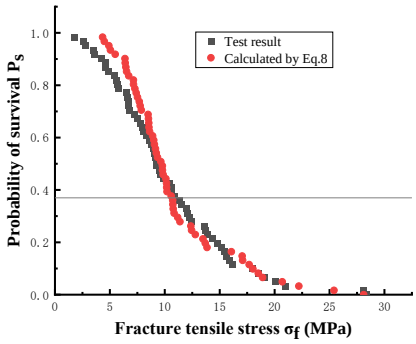

Fig. 8 Force displacement curve of the sample

measured particle strength distributions, this study adopted the same reference point as used in the Weibull distribution. Specifically, the specific fracture energy corresponding to a 37% survival probability was selected as the conversion basis. This value was transformed to match the tensile strength at 37% survival probability, yielding the corresponding stiffness defined as the "equivalent stiffness" $K^{0.}$ For the current tests, K^0 was determined to be 4.7×10^6N/m. Under perfect elasticity, the following relationship holds

$$\sigma_f = \frac{0.9\sqrt{2EK^0}}{d^2} \tag{8}$$

where d is the particle dimension, taken as $d = (d_2\ d_3)\ 1/2$, where d_2 and d_3 are the dimensions of the minimum section of the smallest circumscribable cuboid (SCC) of the particle, that is, the intermediate and minimum diameters.

By applying the equivalent stiffness to all data points in the specific fracture energy distribution shown in Fig. 8, the converted particle strength distribution is presented as red scatter points in Fig. 8.

It should be noted that although both sets of scatter points in Fig. 8 represent the tensile strength distribution of limestone particles, they do not exhibit a one-to-one correspondence. The black data points, obtained experimentally, follow an ascending order of particle tensile strength, while the red data points, derived from the specific fracture energy distribution, are arranged according to increasing specific fracture energy. However, a particle's tensile strength does not directly correlate with its specific fracture energy. Consequently, points sharing the same survival probability *Ps* in both distributions do not necessarily represent the same individual particle and thus lack strict comparability, serving primarily for statistical distribution analysis.

As shown in Fig. 8, the particle strength data points (red) calculated from specific fracture energy using Eq. (8) with equivalent stiffness demonstrate fundamentally similar distribution characteristics to the experimental data (black). However, subtle differences emerge in the low-strength region: the experimentally measured strength distribution appears more uniform with relatively lower values, whereas the processed specific fracture energy distribution shows greater concentration with slightly higher values. This discrepancy may stem from particles with lower specific fracture energy inherently possessing reduced stiffness. The uniform application of an equivalent stiffness value (K^0=4.7×10^6N/m) in Eq. (8), which exceeds the actual stiffness of these particles, could lead to overestimated strength calculations.

Nevertheless, the overall comparison reveals strong agreement: the calculated strength distribution ranges [4.351, 28.196] MPa closely approximates the experimental range [1.773, 28.354] MPa. Moreover, the survival probabilities progressively converge with increasing failure strength, demonstrating the validity of using specific fracture energy data combined with the equivalent stiffness concept for strength prediction. These results confirm the fundamental rationality of assuming perfect elastic behavior with equivalent stiffness in Eq. (8).

7. Conclusions

This study designed and conducted single-particle crushing tests on limestone particles. Using the force-displacement curves obtained from these tests, we performed comprehensive analyses of both particle strength and specific fracture energy for 10-20 mm limestone particles.

1. This study determined the crushing stress distribution characteristics of Baihetan limestone through single-particle crushing tests. The results indicate that the peak strength of 10-20 mm particles ranged from 1.77 to 28.35 MPa. These findings can serve as a benchmark for numerical simulation analysis and provide guidance for engineering practice.
2. This study proposes a novel concept of equivalent stiffness under a perfectly elastic assumption. This theoretical framework was applied to analyze fracture energy data, which was then systematically compared with measured particle strength data. The derived equivalent stiffness parameter effectively addresses deformations prior to particle failure, thereby bridging a gap in the existing research.

Acknowledgements

This research was supported by the National Natural Science Foundation of China (Grant Nos. 51578413) and the Fundamental Research Funds for the Central Universities (Grant No. 2023-2-ZD-08).

The authors declare that they have no known competing financial interests or personal relationships that could have appeared to influence the work reported in this paper.

References

Barrios, G.K.P., de Carvalho, R,M. and Tavares, L.M. (2011), "Modeling breakage of monodispersed particles in unconfined beds", *Miner. Eng.*, **24**, 308-318. https://doi.org/10.1016/j.mineng.2010.09.018.

Cavarretta, I. and O'Sullivan, C. (2012), "The mechanics of rigid irregular particles subject to uniaxial compression", *Géotechnique*, **62**(8), 681-692. https://doi.org/10.1680/geot.10.P.102.

Golewski, G.L. (2024), "Effect of coarse aggregate type on the fracture toughness of ordinary concrete", *Infrastructures*, **9**(10), 185. https://doi.org/10.3390/infrastructures9100185.

Golewski, G.L., Xi, X.Y. and Zheng, YX. (2025), "Experimental evaluation of Mode II fracture and microstructure of matrix-aggregate bond of concrete with crushed limestone", *Case Stud. Constr. Mater.*, **23**, , e05183. https://doi.org/10.1016/j.cscm.2025.e05183.

Gong, J., Cheng, L.P. and Zhao, L.H. (2021), "Study on the packing and shear characteristics of granular mixtures via the DEM", *Geomech. Eng.*, **27**(3), 223-237. https://doi.org/10.12989/gae.2021.27.3.223.

Griffith, A.A. (1921), "The phenomena of rupture and flow in solids", *Philos. T. R. Soc. London A*, **221**(587), 163-198.

Jiang, M.J., Li, T. and Hu, H.J. (2014), "DEM analyses of one-dimensional compression and collapse behaviour of unsaturated structural loess", *Comput. Geotech.*. **60**, 47-60. https://doi.org/10.1016/j.compgeo.2014.04.002.

Lee, D.M. (1992), "The angles of friction of granular fills". PhD thesis, Cambridge University.

Li, R.D., Gao, X., He, S.H., Ru, D. and Ding, Z. (2024), "Fractal analysis of particle size and morphology in single-particle breakage based on 3D images", *Fractal Fractional*, **8**(11), 614. https://www.mdpi.com/2504-3110/8/11/614.

Li, S., Liu, Y., Qian, G., Liu, X. and Wang, H. (2023), "Numerical investigation into particle crushing effects on the shear behavior of gravel", *Geomech. Eng.*, **35**(2), 209-219. https://doi.org/10.12989/gae.2023.35.2.209.

Li, X., Liu,Y.Y. and Qian, G.P. (2023), "Numerical investigation into particle crushing effects on the shear behavior of gravel", *Geomech. Eng.*, **35**(2), 209-219. https://doi.org/10.12989/gae.2023.35.2.209.

Marsal, R.J. (1972), "Mechanical properties of rockfill. In Embankment dam engineering: Casagrande volume (Eds., R.C. Hirschfeld and S.J. Poulos)", New York: Wiley.

Marsal, R.J. (1973), "Mechanical properties of rockfill. In Embankment dam engineering", *Casagrande volume* (Eds., R.C. Hirschfeld and S.J. Poulos), John Wiley & Sons, New York.

McDowell, G.R. and Bolton, M.D. (2000), "On the micromechanics of crushable aggregates", *Géotechnique*, **48**(5), 667-679. https://doi.org/10.1680/geot.1998.48.5.667.

Meng, M.Q., Xiao, Y., Duan, X.Y., Sun, Z., Du, L., Fan, H. and Liu, H. (2022), "Crushing strength of artificial single-particle considering the effect of particle morphology", *Acta Geotechnica*, **17**(9), 3909-3926. https://link.springer.com/article/10.1007/s11440-022-01516-6.

Nakata, Y., Hyde, A.F.L., Hyodo, M. and Murata, H. (1999), "A probabilistic approach to sand crushing in the triaxial test", *Géotechnique*, **49**(5), 567-583. https://doi.org/10.1680/geot.1999.49.5.567.

Nakata, Y., Kato, Y., Hyodo, A.F.L. and Murata, H. (2001), "One-dimensional compression behaviour of uniformly graded sand related to single particle crushing strength", *Soils Found.*, **41**(2), 39~51. https://doi.org/10.3208/sandf.41.2_39.

Penman, A.D.M. and Charles, J.A. (1976), "The quality and suitability of rockfill used in dam construction", *Dams and Embankments*, Practical Studies from the BRE. London: The Construction Press.

Qing, Y., Qiu, Z.F., Tang, Y., Deng, W., Zhang, X., Miu, J. and Song, S. (2022), "Effects of the particle shape and size on the single-particle breakage strength", *Adv. Civil Eng.*, 3386025. https://onlinelibrary.wiley.com/doi/10.1155/2022/3386025.

Sowers, G.F., Williams, R.C. and Wallace, T.S. (1965), "Compressibility of broken rock and settlement of rockfills", *Proceedings of the 6th ICSMFE*, Montreal.

Tavares, L.M. and King, R.P. (1998), "Single-particle fracture under impact loading", *Miner. Process.*, **54**(1), 1-28. https://doi.org/10.1016/S0301-7516(98)00005-2.

Tavares, L.M. and King, R.P. (2002). "Modeling of particle fracture by repeated impacts using continuum damage mechanics", *Powder Technol.*, **123**(2-3), 138-146. https://doi.org/10.1016/S0032-5910(01)00438-7.

Tavares, LM. (2007), "Breakage of single particles: Quasi-static". (Handbook of *Powder Technology*, 2007), https://doi.org/10.1016/S0167-3785(07)12004-2.

Tu, Y., Wang, X., Lan, Y., Wang, J. and Liao, Q. (2022), "Mechanical properties and failure mechanism of gravelly soils in large scale direct shear test using DEM", *Geomech. Eng.*, **30**(1), 27-44. https://doi.org/10.12989/gae.2022.30.1.027.

Veiga Pinto, A.A. (1983), "Previsao do comportamento estrutural de barragens de enrocamento", PhD thesis, *LaboratoÂ rio Nacional de Engenharia Civil*, Lisbon.

Wang, B.X.Y., Zhang, H.H., Qian, J.G. (2025), "Study of wetting behaviors of gravel soil based on specific fracture energy", *J. Test. Eval.*, https://doi.org/10.1520/JTE20240430.

Weibull, W. (1951), "Statistical distribution function of wide applicability", *J. Appl. Mech. ASCE*, **18**(3), 293-297.

Zhou, L., Chu, X., Zhang, X. and Xu, Y. (2016), "Numerical investigations on breakage behaviour of granular materials under triaxial stresses", *Geomech. Eng.*, **11**(5), 639-655. https://doi.org/10.12989/gae.2016.11.5.639.

IC